Materials Advances

ROYAL SOCIETY OF CHEMISTRY

PAPER

View Article Online
View Journal | View Issue

Cite this: *Mater. Adv.*, 2022, 3, 6496

A′–A–π–D–π–A–A′ extended small-molecule photovoltaic donor based on fluorene-diketopyrrolopyrrole with an end-group fluorination effect†

Yang Liu, Lunxiang Yin,* Bao Xie, Chang Liu and Yanqin Li*

Three novel small-molecule donors (SMDs), namely **Flu(DPP)$_2$**, **Flu(DPPsF)$_2$** and **Flu(DPPdF)$_2$**, were designed and synthesized to comprehensively investigate the synergistic effect of extended conjugation and end-group fluorination on photoelectric properties. Firstly, acceptor-π-donor-π-acceptor (A–π–D–π–A) small molecule **Flu(DPP)$_2$** was constructed with alkylated fluorene, ethynyl functionalized thiophene, and diketopyrrolopyrrole (DPP) as the donor, π-bridge bond and acceptor units, respectively. Subsequently, two novel A′–A–π–D–π–A–A′ extended small-molecules **Flu(DPPsF)$_2$** and **Flu(DPPdF)$_2$** were constructed by introducing monofluoro and difluoro substituted phenyl groups at the end group of **Flu(DPP)$_2$**. Compared with **Flu(DPP)$_2$**, **Flu(DPPsF)$_2$** and **Flu(DPPdF)$_2$** show broader absorption. Moreover, due to the introduction of a fluorine substituted phenyl group, the band gap becomes narrower, and difluoro-terminal substituted **Flu(DPPdF)$_2$** shows a narrower electrochemical band gap (E_g^{CV}) than monofluoro-terminal substituted **Flu(DPPsF)$_2$**. More importantly, bulk heterojunction (BHJ) organic photovoltaic (OPV) devices were prepared using **Flu(DPP)$_2$**, **Flu(DPPsF)$_2$** and **Flu(DPPdF)$_2$** as donors mixed with $PC_{61}BM$, respectively. As a result, the devices based on **Flu(DPPsF)$_2$** and **Flu(DPPdF)$_2$** achieve higher power conversion efficiency (PCE) than those based on **Flu(DPP)$_2$**, which are 4.39% and 4.74%, respectively. This work shows that the synergistic strategy with A′–A–π–D–π–A–A′ extended molecular and end-group fluorination provides crucial guidance for the design of novel photovoltaic materials with outstanding photoelectric properties.

Received 6th May 2022,
Accepted 26th June 2022

DOI: 10.1039/d2ma00510g

rsc.li/materials-advances

Introduction

In recent years, organic solar cells (OSCs) have attracted extensive attention because of their flexibility, light-weight and low cost.[1–3] With the innovation and optimization of materials and devices, the power conversion efficiency (PCE) of OSCs has exceeded 20%, showing broad application prospects.[4] As we all know, the active layer is an important component of OSCs.[5,6] Generally, both polymers and small molecules could be used as donor materials in active layers.[7] Compared with polymer donor materials, small molecules have obvious advantages such as well-defined chemical formula, tunable molecular structure, easy purification and high reproducibility.[8–10] However, in recent years, nonfullerene acceptor materials have attracted more attention, and the development of small molecule donor (SMD) materials seems to be relatively lagging behind. Therefore, it is necessary to develop novel SMDs with superior performance and low cost.

Fluorene, a tricyclic fused aromatic compound, has a good planar rigid structure, which is conducive to capturing more photons in the visible and near-infrared wavelengths.[11,12] By introducing fluorene into the molecular structure, the energy band gap of the material can be adjusted and the film-forming property can be improved. At the same time, the solubility of the material can be adjusted by introducing a long side alkyl chain into the fluorene unit.[13,14] Surprisingly, the weak electron-donating ability of fluorene leads to a deeper highest occupied molecular orbital (HOMO) level, which provides great potential for devices to obtain a high open circuit voltage (V_{OC}) based on fluorene as the electron-donating unit.[15–17] For instance, in 2014, the devices based on DCAO3TF composed of fluorene with a high V_{OC} of 1.07 V were obtained by the Chen group,[15] which is one of the highest V_{OC} in OSCs based on the donor/PCBM active layer at that time. Moreover, Hu *et al.* reported three A–D–A SMDs based on a fluorene-core modified by various terminal groups, and then devices based on these materials showed high V_{OC} in the range from 0.97 to 1.07 V.[18] However, the development of organic small molecule donor

School of Chemical Engineering, Dalian University of Technology, Linggong Road 2, Dalian, P. R. China. E-mail: lxyin@dlut.edu.cn, liyanqin@dlut.edu.cn

† Electronic supplementary information (ESI) available: Synthesis, ^{1}H NMR, ^{13}C NMR spectra, HRMS, computational electronic transitions, and CV curve of Fc/Fc$^+$. See DOI: https://doi.org/10.1039/d2ma00510g

materials based on fluorene is still insufficient. In view of the above excellent high V_{OC} properties of fluorene-based small molecules, the construction of organic SMDs containing fluorene is urgently needed at present.

The push–pull conjugated system composed of electron-rich and electron-deficient groups connected by a conjugated π-bridge has been widely used in the design of organic photovoltaic materials.[19,20] Each fragment plays an important role in adjusting the energy level of the molecular orbital and the optical transition of the push–pull system.[21] Among many acceptor units, DPP is outstanding for the following reasons: (a) good planarity;[22] (b) intermolecular interactions, such as hydrogen bonding and π–π interactions, contribute to high charge carrier mobility[23–25] and (c) small molecules based on DPP usually exhibit strong absorption in the visible and even the near-infrared spectrum.[26,27] Therefore, DPP based molecules usually have a narrow band gap and a deep HOMO energy level.[28] The solubility of DPP-based molecules could be increased by alkyl substitution at the 2,5-position of the lactam nitrogen, which is conducive to the formation of good film morphology with fullerene acceptors.[29] Based on these significant advantages, DPP units have great potential in the design of organic photovoltaic materials.

Sometimes minor modifications to the molecular structure can lead to significant improvements in the photovoltaic properties of materials. Therefore, a reasonable modification strategy plays an important role in the innovation of new materials. In order to improve the short-circuit current density (J_{SC}), various modification strategies are used to redshift the absorption spectrum as much as possible, such as expanding the conjugation of the central nucleus to increase its electron donating ability,[30–32] or inserting conjugated fragments between the D-unit and the A-unit.[33–35] In addition, the absorption spectrum of compounds can also be broadened by extending the conjugation of molecules or increasing the electron acceptance ability of the A-unit.[36–40] Fluorine, due to its small atomic radius and high electronegativity, has strong electron-withdrawing properties.[41] The introduction of a fluorine atom into the end group can not only broaden the light absorption and reduce the molecular energy level, but also enhance the interaction between molecules through C–F···H, C–F···S and C–F···π interactions, which are helpful in optimizing the morphology of the active layer.[42–44] However, the systematic research using two or more synergetic strategies still needs to be further explored.

Inspired by the above discussion, three small molecules, namely **Flu(DPP)$_2$**, **Flu(DPPsF)$_2$** and **Flu(DPPdF)$_2$** were designed and synthesized to investigate the extended conjugation and fluorination effects. The molecular design concept and chemical structures of the three compounds are shown in Scheme 1. For comparison, the reference molecule **Flu(DPP)$_2$** was constructed with alkylated fluorene as the donor (D) unit, DPP as the acceptor (A) unit, and ethynyl functionalized thiophene as the π-bridge bond. Subsequently, two novel A′–A–π–D–π–A–A′ extended small-molecules **Flu(DPPsF)$_2$** and **Flu(DPPdF)$_2$** were constructed by introducing monofluoro and difluoro substituted phenyl groups at the end of **Flu(DPP)$_2$**. Density functional theory (DFT) and time-dependent DFT

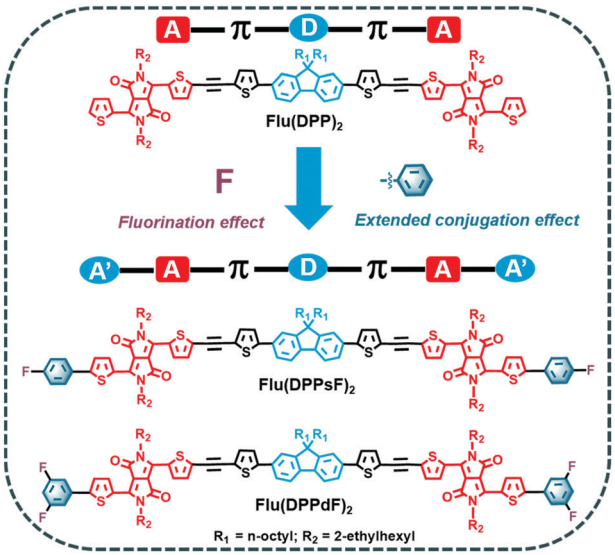

Scheme 1 Molecular design ideas and chemical structures of **Flu(DPP)$_2$**, **Flu(DPPsF)$_2$**, and **Flu(DPPdF)$_2$**.

(TD-DFT) calculations were used to predict the ground-state geometry, energy levels, electron-density distribution, and optical absorption characteristics of the three compounds. Compared with **Flu(DPP)$_2$**, **Flu(DPPsF)$_2$** and **Flu(DPPdF)$_2$** show wider absorption. Moreover, due to the introduction of the fluorine substituted phenyl group, the band gap becomes narrower and difluoro-terminal substituted **Flu(DPPdF)$_2$** shows a narrower electrochemical band gap than monofluoro-terminal substituted **Flu(DPPsF)$_2$**. In addition, **Flu(DPPdF)$_2$** has a deeper HOMO energy level than **Flu(DPPsF)$_2$**, which is expected to obtain high V_{OC} in organic photovoltaic devices (OPVs). It is worth mentioning that the bulk heterojunction (BHJ) OPVs were prepared using **Flu(DPP)$_2$**, **Flu(DPPsF)$_2$** and **Flu(DPPdF)$_2$** as donors mixed with $PC_{61}BM$, respectively. As a result, the devices based on **Flu(DPPsF)$_2$** and **Flu(DPPdF)$_2$** achieve higher power conversion efficiencies (PCEs) than the devices based on **Flu(DPP)$_2$**, which are 4.39% and 4.74% respectively. This work shows that this extended molecular design and fluorine substitution strategy have great potential in the development of new OPV materials.

Experiments and methods

Reagents and materials

All reagents and materials mentioned in this article were purchased from commercial suppliers and can be used directly. Toluene and tetrahydrofuran (THF) were dried with sodium/benzophenone under a nitrogen atmosphere before use.

Device fabrication and characterization

The conventional device structure of ITO/PEDOT:PSS/organic active layer/Al was used to prepare solution-treated BHJ OSCs. Indium tin oxide (ITO) glass substrates were cleaned by ultrasonication for 30 minutes in deionized water, methanol,

acetone, toluene and isopropanol in an appropriate sequence. The substrate was then dried in an infrared oven for 20 minutes. Subsequently, poly(3,4-ethylenedioxy-thiophene):poly(styrene sulfonate) (PEDOT:PSS) was spin-coated on the glass substrate at a rate of 4000 rpm for 60 seconds. After baking at 140 °C for 20 minutes, the glass substrate was transferred to a glove box filled with nitrogen (N_2) for spin-coating of the organic active layer. Subsequently, the mixed solution of the SMDs and $PC_{61}BM$ in chloroform (9 mg mL^{-1}) was spin-coated on the ITO/PEDOT:PSS substrate at 1000 rpm for 60 seconds. Finally, under a vacuum of 10^{-4} Pa, a thin layer of aluminum (80 nm) was deposited on the active layer as the cathode, and eight individual devices with an effective area of 5.0 mm^2 were obtained. The characteristics of hole mobility (μ_h) and electron mobility (μ_e) were obtained by the device structures of the ITO/PEDOT:PSS/organic active layer/Au and ITO/ZnO/organic active layer/Al, respectively. A thin gold layer (80 nm) was deposited on the active layer by thermal evaporation. The zinc oxide (ZnO) dispersion was spin-coated on the glass substrate at a rate of 3000 rpm for 60 seconds. The charge carrier mobility was calculated by the space charge limited current (SCLC) method using the following equation:[45,46] $J = (9/8)\ \varepsilon_0\varepsilon_r\mu\ (V^2/L^3)$, where J, ε_0, ε_r, μ, V and L are the current density, the permittivity of free space, the relative permittivity of the material, the hole mobility and electron mobility, the effective voltage and active layer thickness, respectively.

Measurements and characterization

^{1}H-NMR and ^{13}C-NMR spectra were recorded using a Bruker AVANCE II 500 MHz and a 125 MHz spectrometer with TMS as the internal standard and $CDCl_3$ as the solvent. A MALDI Micro MX spectrometer was used to measure high resolution mass spectra (HRMS). Ultraviolet-visible (UV-Vis) absorption spectra were obtained using an Agilent Cary 5000 spectrometer in $CHCl_3$ solution and in thin films. Cyclic voltammetry (CV) measurements were performed on a CHI610D electrochemical workstation from CH Instruments. Tests were carried out in 0.1 M Bu_4NBF_4/CH_2Cl_2 solution and under a nitrogen atmosphere at a scan rate of 100 mV s^{-1}. Ferrocene–ferrocenium (Fc/Fc^+) was used as an internal standard, and a conventional three-electrode cell with a glassy carbon working electrode, an Ag/Ag^+ (Ag in 0.1 M acetonitrile solution of $AgNO_3$) reference electrode, and a platinum wire counter electrode was used. The HOMO and LUMO energy level value, and the electrochemical band gap were calculated according to the following empirical equations:[47–49] $HOMO^{CV}/LUMO^{CV} = -[E_{OX/red} - E_{1/2}^{ferrocene} + 4.8]$eV, where $E_{1/2}^{ferrocene} = 0.05$ eV *versus* Ag/Ag^+, E_{ox} is the measured onset oxidation potential and E_{red} is the measured onset reduction potential. Thermogravimetric analysis (TGA) was performed using a TA Instruments Q50 thermogravimetric analyzer at a heating rate of 10 °C min^{-1} under nitrogen. The current density–voltage (J–V) characteristics of the OSCs were measured with a computer controlled Keithley 2400 Source Measure Unit under simulated AM 1.5G illumination with an intensity of 100 mW cm^{-2}. The external quantum efficiency (EQE) spectra of OSCs were measured using a solar cell spectral response measurement system QE-R3-011 (Enli Technology Co., Ltd., Taiwan). The J–V characteristics of the hole-only and the electron-only devices were measured with a Keithley 2400 Source Measure Unit system in the dark.

Synthesis and characterization

The synthetic routes for the compounds **Flu(DPP)$_2$**, **Flu(DPPsF)$_2$**, and **Flu(DPPdF)$_2$** are shown in Scheme 2. Compound **1** was prepared according to the previously reported procedures[18] and the synthetic procedure of DPP-based intermediates (compounds **A1**, **A2** and **A3**) can be found in the ESI.†

Synthesis of 2,2′-(9,9-dioctyl-9*H*-fluorene-2,7-diyl) dithiophene (compound 2). A mixture of compound **1** (0.98 g, 1.80 mmol), thiophene-2-boronic acid (553 mg, 4.33 mmol), $Pd(PPh_3)_4$ (42 mg, 0.04 mmol), K_2CO_3 (1.49 g, 10.80 mmol), THF (10 mL) and water (5.4 mL) were refluxed at 85 °C for 24 h under nitrogen. After cooling to room temperature, the reaction solution was poured into water (50 mL) and the resulting mixture was extracted with ethyl acetate (3 × 20 mL). The combined organic layer was dried over anhydrous Na_2SO_4, and then the solvent was removed under reduced pressure. The residue was purified by column

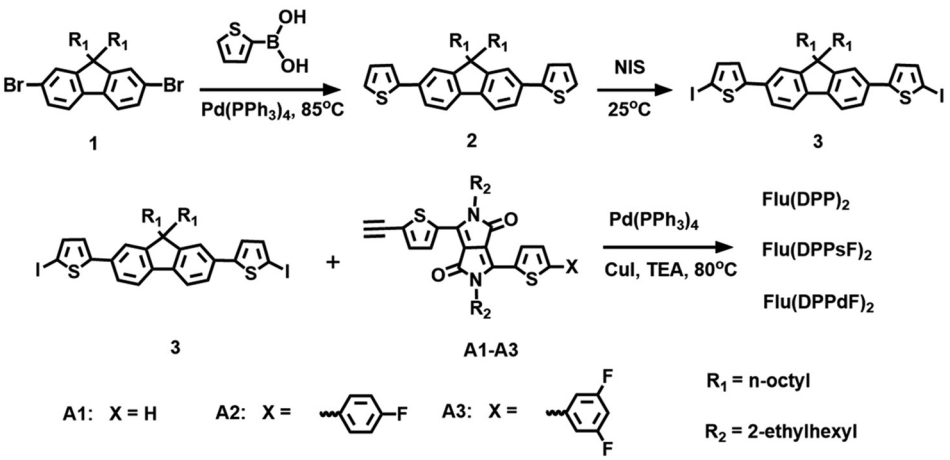

Scheme 2 Synthetic routes for the compounds **Flu(DPP)$_2$**, **Flu(DPPsF)$_2$**, and **Flu(DPPdF)$_2$**.

chromatography on silica gel with petroleum to afford a white liquid (879 mg, 88%). ^{1}H-NMR (500 MHz, $CDCl_3$, ppm): δ 7.68 (d, J = 7.8 Hz, 2H), 7.62 (dd, J_1 = 1.6 Hz, J_2 = 7.8 Hz, 2H), 7.56 (d, J = 1.3 Hz, 2H), 7.39 (dd, J_1 = 1.1Hz, J_2 = 3.6 Hz, 2H), 7.30 (dd, J_1 = 1.1 Hz, J_2 = 5.1 Hz, 2H), 7.11 (dd, J_1 = 3.6 Hz, J_2 = 5.1 Hz, 2H), 2.02 (m, 4H), 1.22–1.02 (m, 20H), 0.79 (t, J = 6.8 Hz, 6H), 0.68 (m, 4H).

Synthesis of 5,5′-(9,9-dioctyl-9*H*-fluorene-2,7-diyl)bis (2-iodothiophene) (compound 3)[50]. A mixture of compound **2** (316 mg, 0.57 mmol), *N*-iodosuccinimide (NIS) (321 mg, 1.43 mmol), chloroform (10 mL), and acetic acid (10 mL) was stirred at room temperature for 5 h in the dark. The reaction solution was neutralized with NaOH (1M), and then $Na_2S_2O_3$ (0.1M) was added to the reaction solution. The resulting solution was extracted with CH_2Cl_2 (3 × 20 mL). The combined organic phase was dried over anhydrous Na_2SO_4, and the solvent was evaporated under reduced pressure. The residue was purified by column chromatography on silica gel with petroleum ether to afford a green liquid (390 mg, 85%). ^{1}H-NMR (500 MHz, $CDCl_3$, ppm) δ 7.67 (d, J = 7.9 Hz, 2H), 7.51 (dd, J_1 = 7.9 Hz, J_2 =1.6 Hz, 2H), 7.45 (d, J = 1.4 Hz, 2H), 7.25 (d, J = 3.8 Hz, 2H), 7.04 (d, J = 3.8 Hz, 2H), 2.01–1.95 (m, 4H), 1.19–1.02 (m, 20H), 0.80 (t, J = 7.0 Hz, 6H), 0.69–0.61 (m, 4H).

Synthesis of Flu(DPP)$_2$. A mixture of compound **3** (218 mg, 0.27 mmol), compound **A1** (356 mg, 0.65 mmol), $Pd(PPh_3)_4$ (30 mg, 0.03 mmol), CuI (10 mg, 0.05 mmol), toluene (15 mL), and TEA (12 mL) was heated at 80 °C for 48 h under nitrogen. After cooling to room temperature, the reaction solution was poured into water (30 mL) and the resulting solution was extracted with CH_2Cl_2 (3 × 20 mL). The collected organic phase was dried over anhydrous Na_2SO_4 and the solvent was removed under reduced pressure. The crude product was purified by silica column chromatography and eluted with petroleum ether/CH_2Cl_2 (1 : 3, v/v) to afford a brown solid (300 mg, 67%). M.p.: 139–141 °C. ^{1}H-NMR (500 MHz, $CDCl_3$, ppm) δ 8.93 (d, J = 3.8 Hz, 2H), 8.91 (d, J = 4.1 Hz, 2H), 7.71 (d, J = 7.9 Hz, 2H), 7.64 (d, J = 5.0 Hz, 2H), 7.60 (d, J = 8.0 Hz, 2H), 7.56 (s, 2H), 7.39 (d, J = 4.1 Hz, 2H), 7.33 (q, J = 3.8 Hz, 4H), 7.30–7.27 (m, 2H), 4.10–3.97 (m, 8H), 2.06–1.98 (m, 4H), 1.95–1.84 (m,4H), 1.41–1.24 (m, 32H), 1.20–1.05 (m, 20H), 0.92–0.85 (m, 24H), 0.80 (t, J = 7.1 Hz, 6H), 0.70 (m, 4H). ^{13}C-NMR (125 MHz, $CDCl_3$, ppm) δ 161.66, 161.61, 152.00, 147.93, 140.79, 140.69, 140.68, 139.24, 135.60, 135.40, 134.03, 132.85, 132.59, 130.82, 129.81, 128.51, 127.92, 125.13, 123.24, 120.99, 120.45, 120.13, 108.79, 108.11, 91.32, 87.05, 55.40, 46.08, 45.97, 40.31, 39.16, 39.10, 31.78, 30.24, 30.23, 30.17, 30.15, 29.94, 29.19, 29.16, 28.37, 28.34, 26.92, 23.78, 23.56, 23.08, 22.60, 14.04, 14.03, 10.50, 10.49. HRMS(MALDI-TOF):1646.7747, [M^+] (calcd for $C_{101}H_{122}N_4O_4S_6$: 1646.7990).

Synthesis of Flu(DPPsF)$_2$. A mixture of compound **3** (194 mg, 0.24 mmol), compound **A2** (340 mg, 0.53 mmol), $Pd(PPh_3)_4$ (25 mg, 0.02 mmol), CuI (8 mg, 0.04 mmol), toluene (15 mL), and TEA (12 mL) was heated at 80 °C for 48 h under nitrogen. After cooling to room temperature, the reaction solution was poured into water (30 mL) and the resulting solution was extracted with CH_2Cl_2 (3 × 20 mL). The collected organic phase was dried over anhydrous Na_2SO_4 and the solvent was evaporated under reduced pressure. The crude product was purified by silica column chromatography and eluted with petroleum ether/CH_2Cl_2(1 : 5, v/v) to give a dark solid (167 mg, 38%). M.p.: 174–175 °C. ^{1}H-NMR (500 MHz, $CDCl_3$, ppm) δ 8.97 (d, J = 4.0 Hz, 2H), 8.91 (d, J = 4.1 Hz, 2H), 7.69 (d, J = 7.9 Hz, 2H), 7.64 (dd, J_1 = 8.6 Hz, J_2 = 5.2 Hz, 4H), 7.61–7.55 (m, 4H), 7.38 (dd, J_1 = 9.8 Hz, J_2 = 4.1 Hz, 4H), 7.33 (q, J = 3.9 Hz, 4H), 7.12 (t, J = 8.5 Hz, 4H), 4.12–3.99 (m, 8H), 2.06–1.99 (m, 4H), 1.97–1.88(m, 4H), 1.41–1.25 (m, 32H), 1.21–1.06 (m, 20H), 0.95–0.87 (m, 24H), 0.80 (t, J = 7.1 Hz, 6H), 0.71 (m, 4H). ^{13}C-NMR (125 MHz, $CDCl_3$, ppm) δ 164.09, 162.10, 161.63, 161.49, 152.00, 148.78, 147.92, 140.78, 140.30, 138.86, 137.14, 135.38, 134.02, 132.85, 132.58, 130.87, 129.47, 128.75, 127.96, 127.89, 127.84, 125.14, 124.50, 123.23, 121.01, 120.46, 120.10, 116.37, 116.19, 108.90, 108.22, 91.37, 87.13, 55.40, 46.13, 46.04, 40.31, 39.25, 39.17, 31.78, 30.37, 30.17, 29.96, 29.20, 29.17, 28.58, 28.35, 28.34, 23.80, 23.71, 23.58, 23.12, 23.10, 22.60, 14.07, 10.58, 10.52. HRMS(MALDI-TOF): 1834.8207, [M^+] (calcd for $C_{113}H_{128}F_2N_4O_4S_6$: 1834.8228).

Synthesis of Flu(DPPdF)$_2$. A mixture of compound **3** (148 mg, 0.18 mmol), compound **A3** (267 mg, 0.40 mmol), $Pd(PPh_3)_4$ (20 mg, 0.02 mmol), CuI (7 mg, 0.03 mmol), toluene (15 mL), and TEA (10 mL) was heated at 80 °C for 48 h under nitrogen. After cooling to room temperature, the reaction solution was poured into water (30 mL) and the resulting solution was extracted with CH_2Cl_2 (3 × 20 mL). The collected organic phase was dried over anhydrous Na_2SO_4 and the solvent was removed by rotary evaporation. The crude product was purified by silica column chromatography and eluted with petroleum ether/CH_2Cl_2 (1 : 4, v/v) to afford a dark solid (175 mg, 51%). M.p.: 228–229 °C. ^{1}H-NMR (500 MHz, $CDCl_3$, ppm) δ 8.93 (dd, J_1 = 7.8 Hz, J_2 = 4.1 Hz, 4H), 7.70 (d, J = 7.9 Hz, 2H), 7.62–7.54 (m, 4H), 7.46 (d, J = 4.0 Hz, 2H), 7.38 (d, J = 4.0 Hz, 2H), 7.33 (d, J = 3.7 Hz, 4H), 7.18 (d, J = 6.0 Hz, 4H), 6.81 (t, J = 8.6 Hz, 2H), 4.12–3.97 (m, 8H), 2.09–1.97 (m, 4H), 1.97–1.84 (m, 4H), 1.48–1.22 (m, 32H), 1.22–1.00 (m, 20H), 0.98–0.85 (m, 24H), 0.80 (t, J = 7.1 Hz, 6H), 0.70 (m, 4H). ^{13}C-NMR (125MHz, $CDCl_3$, ppm) δ 164.47, 164.37, 162.49, 162.38, 161.59, 161.54, 152.01, 148.02, 146.56, 140.81, 139.60, 136.55, 135.76, 134.10, 132.89, 132.58, 130.70, 130.00, 128.30, 125.76, 125.15, 123.26, 120.94, 120.47, 120.13, 109.11, 109.06, 108.95, 108.89, 108.85, 91.61, 87.06, 55.41, 46.17, 46.05, 40.31, 39.31, 39.17, 31.78, 30.39, 30.16, 29.95, 29.20, 29.17, 28.62, 28.34, 28.33, 23.79, 23.72, 23.59, 23.11, 23.10, 22.61, 14.06, 10.57, 10.52. HRMS(MALDI-TOF):1870.8075, [M^+] (calcd for $C_{113}H_{126}F_4N_4O_4S_6$: 1870.8039).

Results and discussion

Synthesis and thermal stability

The synthetic routes of three compounds are summarized in Scheme 2, and the synthetic details of compounds **A1**, **A2** and **A3** can be found in the ESI.† Compound **2** was prepared by the $Pd(PPh_3)_4$-catalyzed Suzuki coupling reaction between compound **1** and thiophene-2-boronic acid, and the yield was 88%. Compound **2** and NIS were treated in a mixture of chloroform and acetic acid to obtain compound **3** with a yield of 85%. The target molecules **Flu(DPP)$_2$**, **Flu(DPPsF)$_2$**, and **Flu(DPPdF)$_2$** were

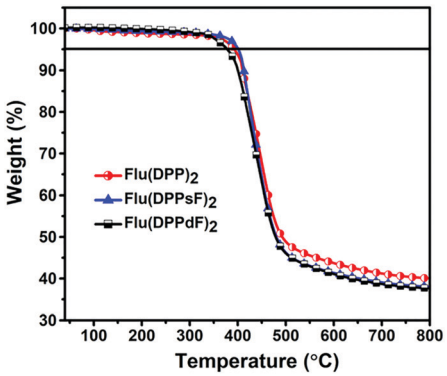

Fig. 1 TGA curves of compounds **Flu(DPP)$_2$**, **Flu(DPPsF)$_2$** and **Flu(DPPdF)$_2$** at a heating rate of 10 °C min^{-1} under a nitrogen flow.

synthesized from compound **3** and compounds **A1**, **A2** and **A3** by the Sonogashira coupling reaction, with yields of 67%, 38%, and 51% respectively. The chemical structures of three target compounds have been fully confirmed by ^{1}H-NMR, ^{13}C-NMR, and MALDI-TOF HRMS. TGA tests were performed on the three compounds to evaluate their thermal stability. As shown in Fig. 1, the decomposition temperatures with 5% weight loss (T_d) of the three compounds are 393 °C for **Flu(DPP)$_2$**, 401 °C for **Flu(DPPsF)$_2$**, and 378 °C for **Flu(DPPdF)$_2$**, indicating that they all have excellent thermal stability.

Theoretical calculations

In order to evaluate the ground state geometry, the electron density distribution, the molecular energy levels and the optical absorption properties of **Flu(DPP)$_2$**, **Flu(DPPsF)$_2$** and **Flu(DPPdF)$_2$**, DFT and TD-DFT calculations were performed using Gaussian09 using the Becke's three-parameter gradient corrected functional (B3LYP) with a polarized 6-31G (d) basis.[51] The longer alkyl chains of the compounds are replaced by methyl to simplify the calculations. The calculation results are shown in Fig. 2. The calculated data of DFT and TD-DFT are shown in Table 1. and the ESI.†

As shown in Fig. 2(a), the dihedral angles of D-π fragments for **Flu(DPP)$_2$**, **Flu(DPPsF)$_2$**, and **Flu(DPPdF)$_2$** are 23.9°, 24.0°, and 25.0°, respectively. The A–A′ units of **Flu(DPPsF)$_2$** and **Flu(DPPdF)$_2$** maintain good planarity with dihedral angles of 25.1° and 23.8°. The appropriate angle can avoid excessive intermolecular stacking, which is more conducive to intramolecular charge transfer (ICT).[52] **Flu(DPPsF)$_2$** and **Flu(DPPdF)$_2$** containing terminal fluorine-substituted phenyl groups are expected to prolong molecular conjugation and enhance the electron-withdrawing ability of terminal groups, resulting in a narrower band gap. The electronic-density distributions and energy levels are shown in Fig. 2(b). The density of the electron cloud of the HOMO is almost distributed in the whole molecule, while the electron cloud density of the lowest unoccupied molecular orbital (LUMO) is more intensive in the DPP and terminal groups with a strong electron-withdrawing ability. Compared with **Flu(DPP)$_2$**, **Flu(DPPsF)$_2$** has a slightly higher HOMO and lower LUMO energy levels, thus reducing the band gap from 2.09 eV to 2.03 eV. The HOMO and LUMO energy levels of **Flu(DPPdF)$_2$** are lower than those of **Flu(DPPsF)$_2$**, which is attributed to the stronger electron-withdrawing capacity of difluoro-substitution than monofluoro-substitution. In addition, the lower HOMO energy level of **Flu(DPPdF)$_2$** may lead to an increase of V_{OC}.

The simulated absorption spectra in chloroform solution and the electronic transition of three molecules are shown in Fig. 2(c). The three molecules exhibit two main absorption bands, one of which belongs to the low-energy region mainly caused by the electronic transition from the HOMO to LUMO, and the other one is located in the high-energy region, which is caused by the electronic transition from the HOMO to LUMO+2 of **Flu(DPP)$_2$**, HOMO to LUMO+4 of **Flu(DPPsF)$_2$** and the HOMO−6 to LUMO of **Flu(DPPdF)$_2$**, respectively. Therefore, it is speculated from the theoretical calculation that the absorption spectra of the three compounds cover the UV-vis and near-infrared region, which indicates that they can show excellent spectral characteristics.

Spectral characteristics

The UV-Vis absorption spectra of the three molecules in chloroform solution and in the thin film state are shown in Fig. 3, and the relevant data are described in Table 1.

In solution, the molar extinction coefficients (ε) of **Flu(DPP)$_2$**, **Flu(DPPsF)$_2$**, and **Flu(DPPdF)$_2$** at the strongest absorption bands are 1.40 × 10^5 M^{-1} cm^{-1}, 0.56 × 10^5 M^{-1} cm^{-1}, and 1.00 × 10^5 M^{-1} cm^{-1}, respectively. Compared with **Flu(DPP)$_2$**, the maximum absorption peaks (λ_{max}^{sol}) of **Flu(DPPsF)$_2$** and **Flu(DPPdF)$_2$** are red-shifted by 30 nm, indicating that the introduction of a fluorine-substituted phenyl group is helpful for capturing more photons. Furthermore, the ε of **Flu(DPPdF)$_2$** is much higher than that of **Flu(DPPsF)$_2$**, indicating that the strategy of difluoro-substitution is helpful in enhancing the absorption of the material.

In the thin film state, the absorption range of three molecules shows an obvious red-shift than in solution, indicating the existence of strong π–π stacking in the solid state.[31,53] According to the equation $E_g^{opt} = 1240/\lambda_{edge}$,[3] the optical band gap (E_g^{opt}) of **Flu(DPP)$_2$**, **Flu(DPPsF)$_2$** and **Flu(DPPdF)$_2$** are 1.80 eV, 1.68 eV, and 1.66 eV, respectively. Compared with **Flu(DPP)$_2$**, the optical band gaps of **Flu(DPPsF)$_2$** and **Flu(DPPdF)$_2$** are narrower, which meets the narrow band gap design of organic small molecule donor materials and helps to improve the J_{SC} of the device.[54]

In order to confirm the aggregation properties of three molecules, temperature-dependent absorption spectra of **Flu(DPP)$_2$**, **Flu(DPPsF)$_2$** and **Flu(DPPdF)$_2$** in dichlorobenzene solutions was obtained, as shown in Fig. 4. When the solution temperature rises from 30 to 80 °C, the ratio of IA_{0-1}/IA_{0-0} for three molecules gradually decreases, indicating that the strong intramolecular aggregation exists in the three molecules. Moreover, the A_{0-1} maximum intensities of **Flu(DPP)$_2$**, **Flu(DPPsF)$_2$** and **Flu(DPPdF)$_2$** showed a certain blue-shift. As a result, the ratio of IA_{0-1}/IA_{0-0} combined with the observed blue-shift suggests that rising temperature leads to molecular disorder and weakens the π–π stacking interactions. However, the shoulder peaks of **Flu(DPPsF)$_2$** and **Flu(DPPdF)$_2$** are more

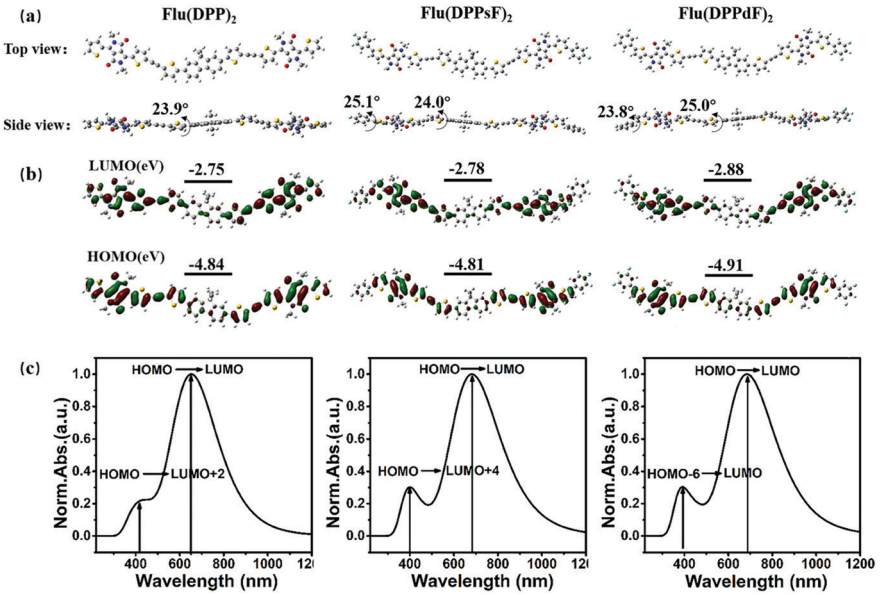

Fig. 2 The summary of the theoretical calculation of **Flu(DPP)$_2$**, **Flu(DPPsF)$_2$**, **Flu(DPPdF)$_2$**: (a) the ground state geometry; (b) electronic-density distributions and energy levels; and (c) predicted optical absorption with the calculated electronic transitions.

Table 1 The photophysical, electrochemical data and theoretically calculated values of **Flu(DPP)$_2$**, **Flu(DPPsF)$_2$**, and **Flu(DPPdF)$_2$**

	UV-Vis absorption				Cyclic voltammetry		DFT calculation	
Compound	λ_{max}^{sol} (nm)/ε (10^5 M^{-1} cm^{-1})	λ_{max}^{film} (nm)	λ_{edge}^{film} (nm)	E_g^{opt} (eV)	$HOMO^{CV}/LUMO^{CV}$ (eV)	E_g^{CV} (eV)	$HOMO^{DFT}/LUMO^{DFT}$ (eV)	E_g^{DFT} (eV)
Flu(DPP)$_2$	584/1.40	615	687	1.80	−5.29/−3.43	1.86	−4.84/−2.75	2.09
Flu(DPPsF)$_2$	614/0.56	667	738	1.68	−5.23/−3.45	1.78	−4.81/−2.78	2.03
Flu(DPPdF)$_2$	614/1.00	674	746	1.66	−5.28/−3.53	1.75	−4.91/−2.88	2.03

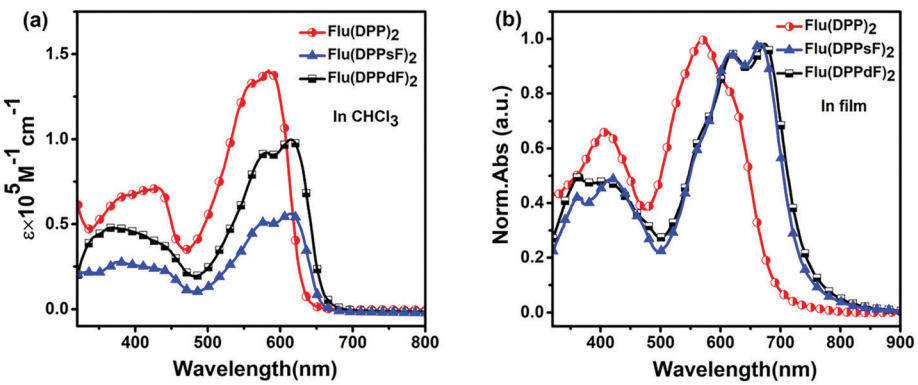

Fig. 3 Spectral characteristics of three compounds: (a) UV-Vis absorption spectra in $CHCl_3$ solution and (b) normalized UV-Vis absorption spectra in the thin film state.

prominent than that of **Flu(DPP)$_2$**, which indicates fluorine substituted **Flu(DPPsF)$_2$** and **Flu(DPPdF)$_2$** can form a stronger and more stable intramolecular aggregation.[55,56]

XRD analysis

The crystallization characteristics of these SMDs were further studied by X-ray diffraction (XRD). The XRD patterns in the thin films of **Flu(DPP)$_2$**, **Flu(DPPsF)$_2$** and **Flu(DPPdF)$_2$** are shown in Fig. 5, the diffraction peaks of **Flu(DPP)$_2$**, **Flu(DPPsF)$_2$** and **Flu(DPPdF)$_2$** are located at 6.58° 6.61° and 6.65°, respectively, indicating three molecules possess good crystallinity.[57] Compared with **Flu(DPP)$_2$**, the diffraction peaks of **Flu(DPPsF)$_2$** and **Flu(DPPdF)$_2$** are stronger and sharper, indicating that the crystallinity of **Flu(DPPsF)$_2$** and **Flu(DPPdF)$_2$** is better. According

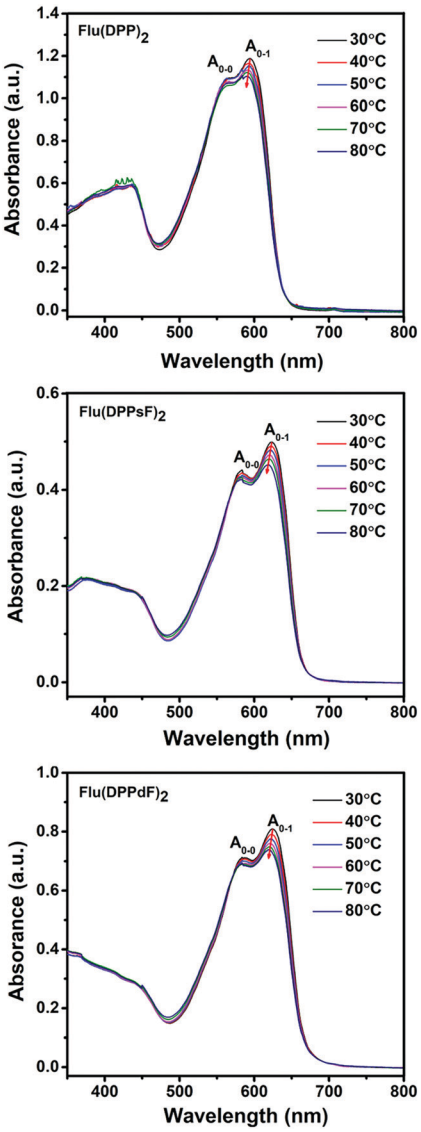

Fig. 4 Temperature-dependent absorption spectra of **Flu(DPP)$_2$**, **Flu(DPPsF)$_2$** and **Flu(DPPdF)$_2$** in dilute *o*-dichlorobenzene solutions.

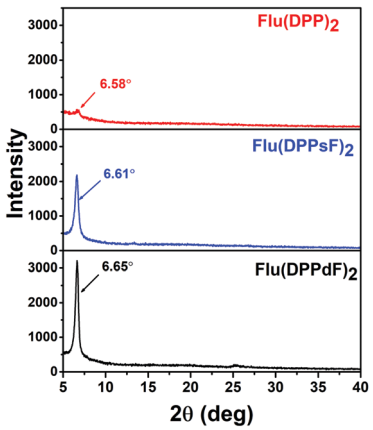

Fig. 5 XRD patterns of the pure **SMDs** films.

to Bragg equation ($2d\sin\theta = n\lambda$), the interplanar spacings of **Flu(DPP)$_2$**, **Flu(DPPsF)$_2$** and **Flu(DPPdF)$_2$** are 13.52 Å, 13.38 Å and 13.29 Å, respectively. The decrease of the spacing indicates that the end-group fluorination can enhance the molecular π–π stacking.[55] The XRD results are in accordance with charge mobility and photovoltaic properties of these SMDs.[58]

Electrochemical properties

Cyclic voltammetry (CV) measurements were performed in order to investigate the electrochemical properties of three compounds. The relevant curves and data are shown in Fig. 6(a) and Table 1. The measured onset reduction potentials and oxidation potentials were −1.32 V/0.54 V, −1.30 V/0.48 V and −1.22 V/0.53 V for **Flu(DPP)$_2$**, **Flu(DPPsF)$_2$** and **Flu(DPPdF)$_2$**, respectively. According to the following empirical equations:[47–49] $\mathrm{HOMO}^{\mathrm{CV}}/\mathrm{LUMO}^{\mathrm{CV}} = -[E_{\mathrm{OX/red}} - E_{1/2}^{\mathrm{ferrocene}} + 4.8]$ eV, where $E_{1/2}^{\mathrm{ferrocene}} = 0.05$ eV the calculated HOMO and LUMO energy levels from the oxidation and reduction potentials are −5.29 eV/−3.43 eV for **Flu(DPP)$_2$**, −5.23 eV/−3.45 eV for **Flu(DPPsF)$_2$**, −5.28 eV/−3.53 eV for **Flu(DPPdF)$_2$**. In addition, the band gaps of **Flu(DPPsF)$_2$** and **Flu(DPPdF)$_2$** are narrower than that of **Flu(DPP)$_2$**, which is consistent with the trend given in the previous theoretical calculation.[27] Compared with **Flu(DPPsF)$_2$**, the lower HOMO level of **Flu(DPPdF)$_2$** helps to obtain higher V_{OC} in OPV devices,[59] which is due to the stronger electron-withdrawing characteristics caused by terminal difluoro-substitution. In short, the variation trends of energy levels and band gaps of the three molecules obtained from CV experiments and theoretical calculations are basically consistent, indicating that theoretical calculations can provide important information for molecular design.

As shown in Fig. 6(b), the HOMO and LUMO energy levels of three molecules as donor materials match well with $PC_{61}BM$, and the LUMO energy level difference with $PC_{61}BM$ exceeds 0.3 eV, which provides sufficient driving force for charge separation at the interface.[60] The results show that the three molecules meet the requirements of photovoltaic materials as donors, which provides conditions for the preliminary study of photovoltaic devices.

Photovoltaic properties

Solution-processed BHJ devices composed of ITO/PEDOT:PSS/SMDs:$PC_{61}BM$/Al were prepared to evaluate the photovoltaic characteristics of new materials. The *J*–*V* curves and related photoelectric parameters are summarized in Fig. 7(a) and Table 2. Without any optimization, the PCEs of devices based on **Flu(DPP)$_2$**, **Flu(DPPsF)$_2$**, and **Flu(DPPdF)$_2$** reached 2.90%, 4.39% and 4.74% respectively. Compared with **Flu(DPP)$_2$**-based devices, the PCEs of the devices based on **Flu(DPPsF)$_2$**, and **Flu(DPPdF)$_2$** increased by 51.4% and 63.4%, respectively, mainly due to the increase of J_{SC} and FF. In addition, compared with the **Flu(DPPsF)$_2$**-based device with a V_{OC} of 0.81 V, **Flu(DPPdF)$_2$**-based devices show a higher V_{OC} of 0.86 V, which indicates that the design of difluoro-substituted materials is better.[3] In short, these results prove the rationality of molecular design strategy.

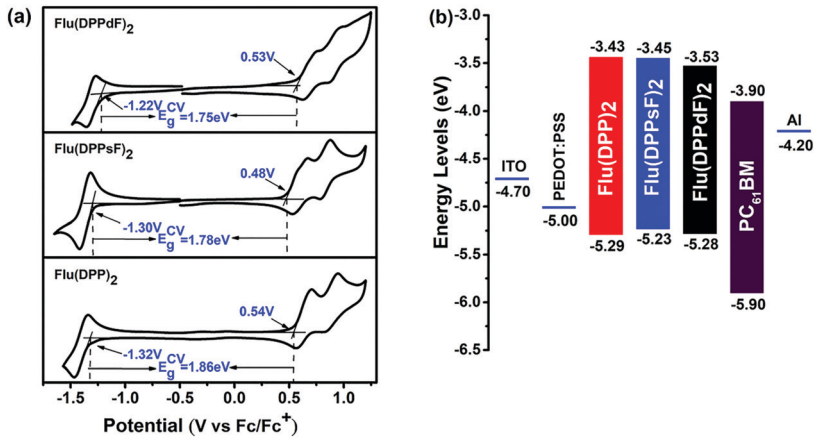

Fig. 6 The CV curves and energy levels: (a) CV curves of **Flu(DPP)$_2$**, **Flu(DPPsF)$_2$** and **Flu(DPPdF)$_2$** in 0.1 M Bu_4NBF_4/CH_2Cl_2 solution at a scan rate of 100 mV s^{-1} under nitrogen; (b) Energy level diagram of **Flu(DPP)$_2$**, **Flu(DPPsF)$_2$**, **Flu(DPPdF)$_2$** and $PC_{61}BM$.

External quantum efficiency

The external quantum efficiency (EQE) curves of devices based on different active layer materials are shown in Fig. 7(b). All devices based on three molecules exhibit two characteristic photon-to-electron response bands, ranging from 300 nm to 750 nm. It is worth noting that in the short wavelength region (300–500 nm), the device based on **Flu(DPPdF)$_2$** has a maximum EQE value of 82.7%, while in the long wavelength region (500–750 nm), the device based on **Flu(DPPsF)$_2$** shows a maximum EQE value of 47.8%. Obviously, the devices based on **Flu(DPPsF)$_2$** and **Flu(DPPdF)$_2$** show a broader and stronger photon–electron response than devices based on **Flu(DPP)$_2$**. The integrated current (J_{SC}^{cal}) of devices based on **Flu(DPP)$_2$**, **Flu(DPPsF)$_2$**, and **Flu(DPPdF)$_2$** obtained from EQE curves are 9.83 mA cm^{-2}, 11.91 mA cm^{-2} and 12.28 mA cm^{-2}, respectively, which are basically consistent with the J_{SC} obtained by J–V measurements (error less than 5%). Based on the above analysis, it can be concluded that the devices based on **Flu(DPPsF)$_2$** and **Flu(DPPdF)$_2$** show more effective photon-to-electron response than the devices based on **Flu(DPP)$_2$**. Therefore, the molecular design of extending the conjugated structure and fluorine-substitution is successful.

Charge carrier transport

In order to further understand the difference in the photovoltaic performance of devices based on three materials **Flu(DPP)$_2$**, **Flu(DPPsF)$_2$**, and **Flu(DPPdF)$_2$**, the charge carrier mobility was tested by the space charge limited current (SCLC) method.

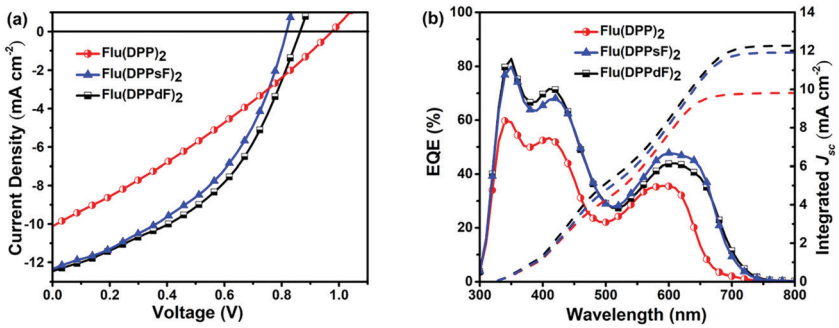

Fig. 7 Photovoltaic characteristics of the devices based on the organic active layer of **Flu(DPP)$_2$**:$PC_{61}BM$, **Flu(DPPsF)$_2$**:$PC_{61}BM$ and **Flu(DPPdF)$_2$**:$PC_{61}BM$, respectively. (a) J–V curves of devices based on the above different active layer materials and (b) EQE spectra and integrated current curves of the devices with different active layer materials.

Table 2 Photovoltaic data of the devices based on the organic active layer with **Flu(DPP)$_2$**:$PC_{61}BM$, **Flu(DPPsF)$_2$**:$PC_{61}BM$, and **Flu(DPPdF)$_2$**:$PC_{61}BM$, respectively

Organic active layer of devices	V_{OC} (V)	J_{SC} (mA cm^{-2})	J_{SC}^{cal} (mA cm^{-2})	FF (%)	PCE (PCE_{ave}) (%)	μ_h (cm^2 V^{-1} s^{-1})	μ_e (cm^2 V^{-1} s^{-1})	μ_h/μ_e
Flu(DPP)$_2$:$PC_{61}BM$	0.97	10.13	9.83	29.51	2.90 (2.67)	3.17×10^{-5}	1.65×10^{-5}	1.92
Flu(DPPsF)$_2$:$PC_{61}BM$	0.81	12.39	11.91	43.74	4.39 (4.08)	7.26×10^{-5}	6.08×10^{-5}	1.19
Flu(DPPdF)$_2$:$PC_{61}BM$	0.86	12.41	12.28	44.41	4.74 (4.33)	1.40×10^{-4}	1.60×10^{-4}	0.88

The average data of PCE are obtained from 24 devices.

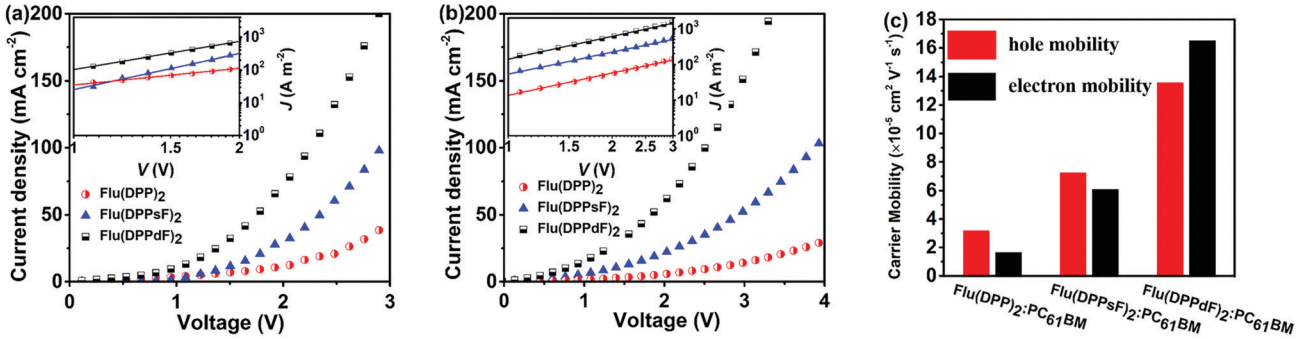

Fig. 8 *J*–*V* curves of the devices in the dark based on the organic active layer with **Flu(DPP)$_2$**:PC$_{61}$BM, **Flu(DPPsF)$_2$**:PC$_{61}$BM and **Flu(DPPdF)$_2$**:PC$_{61}$BM, respectively. (a) The hole-only devices and (b) the electron-only devices. Inset: The *J*–*V* plots in a double logarithmic scale and the solid lines are fit to the data points to an SCLC model. (c) Histogram of the carrier mobility for the devices.

Hole mobility (μ_h) and electron mobility (μ_e) were measured with the device architectures of ITO/PEDOT:PSS/organic active layer/Au and ITO/ZnO/organic active layer/Al, respectively. The charge carrier mobility, *J*–*V* curves and the related data are shown in Fig. 8 and Table 2. As a result, the μ_h values of the device based on **Flu(DPP)$_2$**, **Flu(DPPsF)$_2$**, and **Flu(DPPdF)$_2$** are 3.17×10^{-5}, 7.26×10^{-5} and 1.40×10^{-4} cm^2 V^{-1} s^{-1}, the corresponding μ_e values are 1.65×10^{-5}, 6.08×10^{-5} and 1.60×10^{-4} cm^2 V^{-1} s^{-1} respectively. The devices based on **Flu(DPPsF)$_2$** and **Flu(DPPdF)$_2$** show a higher hole mobility and electron mobility than devices based on **Flu(DPP)$_2$**. In particular, the device based on **Flu(DPPdF)$_2$** shows the highest carrier mobility values. The ratios of μ_h/μ_e of devices based on **Flu(DPP)$_2$**, **Flu(DPPsF)$_2$**, and **Flu(DPPdF)$_2$** are 1.92, 1.19 and 0.88 respectively. The higher short-circuit J_{sc} and PCEs of devices based on **Flu(DPPdF)$_2$** benefit from its higher and more balanced μ_h/μ_e value.[24,61] In addition, the contact angle of **Flu(DPPdF)$_2$** is most similar to those of PC$_{61}$BM (Fig. S11 in the ESI†), indicating that there is the most appropriate miscibility between **Flu(DPPdF)$_2$** and PC$_{61}$BM, which could be helpful for the formation of excellent bulk heterojunction (BHJ) morphology.[57,62]

Conclusions

In conclusion, three new small molecule donors have been designed and synthesized successfully. In particular, two novel A′–A–π–D–π–A–A′ extended small-molecules **Flu(DPPsF)$_2$** and **Flu(DPPdF)$_2$** were constructed by introducing monofluoro and difluoro substituted phenyl groups at the end group of **Flu(DPP)$_2$**. The synergistic effect of extended conjugation and end-group fluorination on photovoltaic properties were investigated comprehensively. It is worth mentioning that devices based on **Flu(DPPsF)$_2$** and **Flu(DPPdF)$_2$** achieved a higher PCE of 4.39% and 4.74%, respectively, compared with **Flu(DPP)$_2$**. This is mainly because these two extended fluorine-substituted materials based on **Flu(DPPsF)$_2$** and **Flu(DPPdF)$_2$** exhibit broader light absorption, narrower band gap and better crystallinity. Moreover, the devices based on these two materials show more effective photon–electron response, higher and more balanced carrier transport characteristics. This work shows that the synergistic strategy with A′–A–π–D–π–A–A′ extended molecular and fluorine-substitution provides crucial guidance for the design of novel materials with improved photovoltaic performance.

Conflicts of interest

There are no conflicts to declare.

Acknowledgements

To the authors thank the support of the National Natural Science Foundation of China (No. 21102013) and the Scientific Research Foundation Project of Central Universities (DUT16ZD205).

Notes and references

1 H. Chen, D. Hu, Q. Yang, J. Gao, J. Fu, K. Yang, H. He, S. Chen, Z. Kan, T. Duan, C. Yang, J. Ouyang, Z. Xiao, K. Sun and S. Lu, *Joule*, 2019, **3**, 3034–3047.
2 R. Sun, Y. Wu, X. Yang, Y. Gao, Z. Chen, K. Li, J. Qiao, T. Wang, J. Guo, C. Liu, X. Hao, H. Zhu and J. Min, *Adv. Mater.*, 2022, 2110147.
3 X. He, L. Yin and Y. Li, *New J. Chem.*, 2019, **43**, 6577–6586.
4 Z. Zheng, J. Wang, P. Bi, J. Ren, Y. Wang, Y. Yang, X. Liu, S. Zhang and J. Hou, *Joule*, 2022, **6**, 171–184.
5 X. He, L. Yin and Y. Li, *J. Mater. Chem. C*, 2019, **7**, 2487–2521.
6 K. Wang, Y. Li and Y. Li, *Macromol. Rapid Commun.*, 2020, **41**, 1900437.
7 Y. Liu, B. Liu, C. Q. Ma, F. Huang, G. Feng, H. Chen, J. Hou, L. Yan, Q. Wei, Q. Luo, Q. Bao, W. Ma, W. Liu, W. Li, X. Wan, X. Hu, Y. Han, Y. Li, Y. Zhou, Y. Zou, Y. Chen, Y. Li, Y. Chen, Z. Tang, Z. Hu, Z. G. Zhang and Z. Bo, *Sci. China: Chem.*, 2022, **65**, 224–268.
8 T. Xu, J. Lv, K. Yang, Y. He, Q. Yang, H. Chen, Q. Chen, Z. Liao, Z. Kan, T. Duan, K. Sun, J. Ouyang and S. Lu, *Energy Environ. Sci.*, 2021, **14**, 5366–5376.
9 B. Kan, Y. Kan, L. Zuo, X. Shi and K. Gao, *InfoMat*, 2021, **3**, 175–200.

10 X. Zhang, L. Qin, Y. Li, J. Yu, H. Chen, X. Gu, Y. Wei, X. Lu, F. Gao, H. Huang, X. Zhang, L. Qin, H. Chen, X. Gu, Y. Wei, H. Huang, Y. Li, X. Lu, J. Yu and F. Gao, *Adv. Funct. Mater.*, 2022, 2112433.
11 B. Yadagiri, K. Narayanaswamy, S. Revoju, B. Eliasson, G. D. Sharma and S. P. Singh, *J. Mater. Chem. C*, 2019, **7**, 709–717.
12 X. X. Dai, H. L. Feng, Z. S. Huang, M. J. Wang, L. Wang, D. Bin Kuang, H. Meier and D. Cao, *Dyes Pigm.*, 2015, **114**, 47–54.
13 R. Abbel, A. P. H. J. Schenning and E. W. Meijer, *J. Polym. Sci., Part A: Polym. Chem.*, 2009, **47**, 4215–4233.
14 J. U. Wallace and S. H. Chen, *Adv. Polym. Sci.*, 2008, **212**, 145–186.
15 W. Ni, M. Li, B. Kan, Y. Zuo, Q. Zhang, G. Long, H. Feng, X. Wan and Y. Chen, *Org. Electron.*, 2014, **15**, 2285–2294.
16 I. Ljubić and A. Sabljić, *J. Phys. Chem. A*, 2011, **115**, 4840–4850.
17 K. Ramki, N. Venkatesh, G. Sathiyan, R. Thangamuthu and P. Sakthivel, *Org. Electron.*, 2019, **73**, 182–204.
18 C. Hu, L. Yin, B. Xie and Y. Li, *Dyes Pigm.*, 2020, **183**, 108709.
19 F. Bureš, *RSC Adv.*, 2014, **4**, 58826–58851.
20 Y. Patil, R. Misra, F. C. Chen, M. L. Keshtov and G. D. Sharma, *RSC Adv.*, 2016, **6**, 99685–99694.
21 V. Malytskyi, J. J. Simon, L. Patrone and J. M. Raimundo, *RSC Adv.*, 2015, **5**, 354–357.
22 Y. Patil and R. Misra, *J. Mater. Chem. C*, 2019, **7**, 13020–13031.
23 H. Shi, Z. Gu, X. Gu, H. Pan, J. Pan, X. Hu, C. Fan, M. Shi and H. Chen, *Synth. Met.*, 2014, **188**, 66–71.
24 W. Lee, J. Choi and J. W. Jung, *Dyes Pigm.*, 2019, **161**, 283–287.
25 C. B. Nielsen, M. Turbiez and I. McCulloch, *Adv. Mater.*, 2013, **25**, 1859–1880.
26 B. Sun, W. Hong, Z. Yan, H. Aziz and Y. Li, *Adv. Mater.*, 2014, **26**, 2636–2642.
27 F. Cheng, X. He, L. Yin, B. Xie and Y. Li, *Dyes Pigm.*, 2020, **176**, 108211.
28 W. Li, W. S. C. Roelofs, M. M. Wienk and R. A. J. Janssen, *J. Am. Chem. Soc.*, 2012, **134**, 13787–13795.
29 D. Molina, M. J. Álvaro-Martins and Á. Sastre-Santos, *J. Mater. Chem. C*, 2021, **9**, 16078–16109.
30 J. Wu, Q. Liu, L. Ye, X. Guo, Q. Fan, J. Lv, M. Zhang and W. Y. Wong, *Energy Fuels*, 2021, **35**, 19061–19068.
31 B. Xie, L. Yin, J. Fan, C. Liu and Y. Li, *J. Mater. Chem. C*, 2022, **10**, 3248–3258.
32 B. Jia, S. Dai, Z. Ke, C. Yan, W. Ma and X. Zhan, *Chem. Mater.*, 2018, **30**, 239–245.
33 B. Zhao, W. Wang, Z. Cong, L. Wang, H. Wu, S. Liu and C. Gao, *ACS Appl. Energy Mater.*, 2021, **4**, 4119–4128.
34 L. Wang, L. Yin, C. Ji, Y. Zhang, H. Gao and Y. Li, *Org. Electron.*, 2014, **15**, 1138–1148.
35 Z. Jia, S. Qin, L. Meng, Q. Ma, I. Angunawela, J. Zhang, X. Li, Y. He, W. Lai, N. Li, H. Ade, C. J. Brabec and Y. Li, *Nat. Commun.*, 2021, **12**, 1–10.
36 F. Cheng, X. He, L. Yin, B. Xie and Y. Li, *Dyes Pigm.*, 2020, **176**, 108211.
37 J. Pan, Y. Shi, J. Yu, H. Zhang, Y. Liu, J. Zhang, F. Gao, X. Yu, K. Lu and Z. Wei, *ACS Appl. Mater. Interfaces*, 2021, **13**, 22531–22539.
38 W. Zhao, S. Li, H. Yao, S. Zhang, Y. Zhang, B. Yang and J. Hou, *J. Am. Chem. Soc.*, 2017, **139**, 7148–7151.
39 Abdullah, S. Ameen, M. S. Akhtar, L. Fijahi, E. B. Kim and H. S. Shin, *Opt. Mater.*, 2019, **91**, 425–432.
40 Suman, A. Bagui, A. Garg, B. Tyagi, V. Gupta and S. P. Singh, *Chem. Commun.*, 2018, **54**, 4001–4004.
41 M. Li, G. Zhang, L. Xiong, M. Zhu, Y. Pei, Q. Peng and Y. Liu, *Dyes Pigm.*, 2018, **158**, 402–411.
42 N. Qiu, C. Liu, H. Lang, J. Xu, R. Su, J. Jiang, J. Tian and J. Li, *New J. Chem.*, 2022, **46**, 8500–8506.
43 Q. Wu, D. Deng, J. Zhang, W. Zou, Y. Yang, Z. Wang, H. Li, R. Zhou, K. Lu and Z. Wei, *Sci. China: Chem.*, 2019, **62**, 837–844.
44 D. Fan, C. Fan, H. Fan, S. Bao, Y. Zheng, H. Yang, X. Zhu, C. Cui and Y. Li, *Mol. Syst. Des. Eng.*, 2021, **6**, 739–747.
45 P. Blom, M. de Jong and M. van Munster, *Phys. Rev. B: Condens. Matter Mater. Phys.*, 1997, **55**, R656.
46 K. Shi, B. Qiu, C. Zhu, J. Yao, X. Xia, J. Zhang, L. Meng, S. Huang, X. Lu, Y. Wan, Z. G. Zhang and Y. Li, *ACS Appl. Mater. Interfaces*, 2021, **13**, 54237–54245.
47 H. Gao, Y. Li, L. Wang, C. Ji, Y. Wang, W. Tian, X. Yang and L. Yin, *Chem. Commun.*, 2014, **50**, 10251–10254.
48 C. Ji, L. Yin, L. Wang, T. Jia, S. Meng, Y. Sun and Y. Li, *J. Mater. Chem. C*, 2014, **2**, 4019–4026.
49 Z. Li, Y. Zhang, A. L. Holt, B. P. Kolasa, J. G. Wehner, A. Hampp, G. C. Bazan, T.-Q. Nguyen and D. E. Morse, *New J. Chem.*, 2011, **35**, 1327–1334.
50 S. Kawasaki, J. Ujita, K. Toyota and M. Yoshifuji, *Chem. Lett.*, 2005, **34**, 724–725.
51 L. Wang, L. Yin, L. Wang, B. Xie, C. Ji and Y. Li, *Dyes Pigm.*, 2017, **140**, 203–211.
52 Jiali Song, Xiaonan Xue, Bingbing Fan, Lijun Huo and Yanming Sun, *Mater. Chem. Front.*, 2018, **2**, 1626–1630.
53 C. Ye, Y. Wang, Z. Bi, X. Guo, Q. Fan, J. Chen, X. Ou, W. Ma and M. Zhang, *Org. Electron.*, 2018, **53**, 273–279.
54 D. Meng, R. Zheng, Y. Zhao, E. Zhang, L. Dou and Y. Yang, *Adv. Mater.*, 2022, **34**, 2107330.
55 M. Li, Z. Qiu, G. Zhang, Y. Liu, L. Xiong, D. Bai, M. Zhu, Q. Peng and W. Zhu, *J. Mater. Chem. A*, 2018, **6**, 12493–12505.
56 Z. Qiu, X. Xu, L. Yang, Y. Pei, M. Zhu, Q. Peng and Y. Liu, *Sol. Energy*, 2018, **161**, 138–147.
57 M. Li, S. Wang, C. Bao, Z. Liu, D. Bai, Z. Yang, W. Zhu, Q. Peng and Y. Liu, *J. Mater. Chem. C*, 2019, **7**, 12217–12230.
58 Z. Qiu, X. Xu, S. Zhang, P. Wang, Y. Wang, Y. Pei, Q. Peng and Y. Liu, *Dyes Pigm.*, 2017, **147**, 505–513.
59 Q. Fan, Z. Xu, X. Guo, X. Meng, W. Li, W. Su, X. Ou, W. Ma, M. Zhang and Y. Li, *Nano Energy*, 2017, **40**, 20–26.
60 T. Xu, J. Lv, K. Yang, Y. He, Q. Yang, H. Chen, Q. Chen, Z. Liao, Z. Kan, T. Duan, K. Sun, J. Ouyang and S. Lu, *Energy Environ. Sci.*, 2021, **14**, 5366–5376.
61 Y. Un Kim, G. Eun Park, S. Choi, D. Hee Lee, M. Ju Cho and D. H. Choi, *J. Mater. Chem. C*, 2017, **5**, 7182–7190.
62 Y. Wang, S. Dong, Y. Miao, D. Li, W. Qin, H. Cao, L. Yang, L. Li and S. Yin, *IEEE J. Photovoltaics*, 2017, **7**, 550–557.